



Gas detection using cavity-enhanced Raman spectroscopy with a bidirectional multi-pass cell and polarization beam-splitting optical path

Yuhao Zheng¹ · Xiaer Zou¹ · Sailing He^{1,2}

Received: 13 May 2024 / Accepted: 16 July 2024 / Published online: 24 July 2024
© The Author(s) 2024

Abstract

We demonstrate a substantial enhancement of gas Raman scattering using a bidirectional multi-pass cavity CERS system, which incorporates a polarization beam-splitting optical path. The system design allows the laser light to traverse the multi-pass cavity for four specific trips, satisfying the need for quick detection of various gas components. Our gas detection experiments using multi-pass cavities with different times of reflection indicate that the addition of polarization beam-splitting optical path gives 1.5 to 1.68 times enhancement of Raman signal compared with that of the system without polarization beam-splitting. For the detection of CH₄, a limit of detection of 1.66 ppm was achieved with our system using a multi-pass cell with 41 times of reflection and an integration time of 30s. Our proposed design, which integrates a bidirectional multi-pass cavity with polarization beam-splitting optical path, gives an economical multicomponent gas detection system and a valuable tool for guiding the design and precise alignment of these cavities. This system shows significant promise for applications in e.g. human breath and environmental monitoring.

1 Introduction

The concurrent detection of multi-component gases holds critical importance across diverse sectors, including environmental, medical, and industrial applications [1–4]. Gas detection technologies are broadly categorized into optical and non-optical methods. Optical detection methods primarily use spectroscopic techniques to ascertain gas types and concentrations. Conventional spectroscopic methods, such as infrared absorption [5], photoacoustic [6–8], and cavity ring-down spectroscopy [9], have been extensively utilized for gas detection, offering commendable sensitivity and results. However, these methods typically require the

use of lasers with multiple wavelengths or costly broadband lasers to detect multi-component gases [10]. Furthermore, infrared spectroscopy faces challenges in detecting homonuclear diatomic gases like N₂ and H₂.

Raman spectroscopy presents an alternative technique for gas sensing, leveraging the Raman scattering phenomenon intrinsic to gas [11]. This method enables the identification of gas types and concentrations through the analysis of Raman scattering spectra's intensity. It is capable of utilizing a singular wavelength light to concurrently detect multiple gas components, including the ability to sense homonuclear diatomic gases. Consequently, Raman spectroscopy serves as a potent instrument for the simultaneous detection of various gas constituents, applicable across multiple domains. However, the inherently weak Raman scattering cross section of gas molecules necessitates the employment of strategies to amplify the Raman signal for high sensitivity gas detection.

Presently, the enhancement of gas Raman scattering is predominantly facilitated by fiber-enhanced Raman spectroscopy (FERS) [12–14] and cavity-enhanced Raman spectroscopy (CERS) [15–20]. FERS employs a hollow-core fiber to extend the laser's interaction path with the test substance, thereby augmenting the Raman signal's collection

✉ Sailing He
sailing@kth.se

¹ Centre for Optical and Electromagnetic Research, Zhejiang Provincial Key Laboratory for Sensing Technologies, College of Optical Science and Engineering, National Engineering Research Center for Optical Instruments, Zhejiang University, Hangzhou 310058, China

² Department of Electromagnetic Engineering, School of Electrical Engineering, KTH Royal Institute of Technology, Stockholm SE-100 44, Sweden

efficiency and amplifying its intensity. This technique has proven to enhance Raman signals effectively, achieving sensitivities at the parts-per-million (ppm) level. Conversely, the Fabry-Perot cavity enhancement [16, 18] intensifies the laser power within an optical resonant cavity, significantly bolstering Raman scattering and sensitivity. Moreover, multiple-pass cavity enhancement [15, 17, 19], utilizing multi-pass cells, either prolongs the laser's interaction with the gas or amplifies the laser power at the focal point to improve Raman scattering. This approach, while structurally straightforward, also attains high detection sensitivity. Multi-pass CERS systems are categorized into side detection [3, 21] and collinear geometries [22] based on their light collection methodologies. Collinear geometry requires multi-pass cavities that reflect the laser beam along its entry path. While potentially accruing more background noise than side collection, this modality secures more Raman signals. Additionally, the overlap of laser beams in multi-pass cavities is less critical than in side detection setups [22, 23]. Resonance Raman spectroscopy has also been utilized in some biomedical and environmental detections [24–26].

In this work, we devised an enhancement system for gas Raman detection, integrating bidirectional multi-pass cavities with a polarization beam-splitting optical path to detect ambient air. The innovative design allows the laser beam circulate four trips within the multi-pass cavity, amplifying the Raman scattering intensity by an estimated factor of 1.6 relative to conventional collinear detection CERS systems under identical conditions. Moreover, we introduce a precise vector-based methodology to compute the light trajectory within the multi-pass cavity. Employing this method,

we engineered multi-pass cavities featuring varying reflection number and evaluated their corresponding Raman scattering enhancement factors.

2 Experimental section

Figures 1 and 2 illustrates the collinear collection CERS gas system. A continuous-wave solid-state laser, with a maximum power of 2 W and a linewidth less than 0.2 nm at 532 nm, functions as the system's light source. The laser beam output exhibits a polarization ratio exceeding 100:1, a beam diameter of 3 mm, and a beam divergence angle less than 1.2 mrad. To safeguard the laser from potential damage caused by the reflected light, a high-power optical isolator (OI), with a transmittance rate of 89% at the 532 nm, has been positioned at the laser's forefront.

The S-Polarized laser beam traverses the polarizing beam splitter (PBS), transitioning from linear polarization to circular polarization via the quarter-wave plate (QW). Given the high transmission of 97.21% for the PBS and 99.8% for the QW, the loss impact of these components on the laser power is minimal. The laser is then reflected by a long-pass dichroic mirror (DM). To preserve the laser polarization state post-reflection, a zero-phase shift dichroic mirror corresponding to the wavelength is chosen. An achromatic lens (AL_1) with a focal length of 150 mm is employed to focus the laser into the near concentric multi-pass cell. This multi-pass cell consists of two concave spherical mirrors (SM_1 SM_2) with a diameter of 25.4 mm and a focal length of 25 mm. The spherical mirror boasts a reflectivity of 99.6%

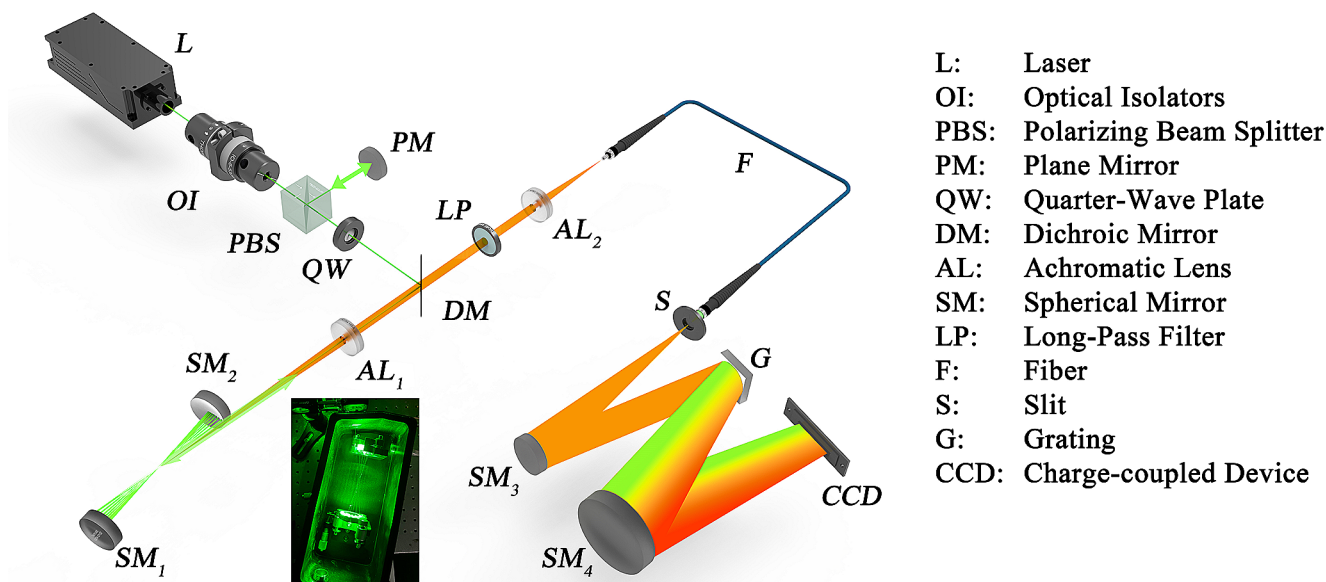
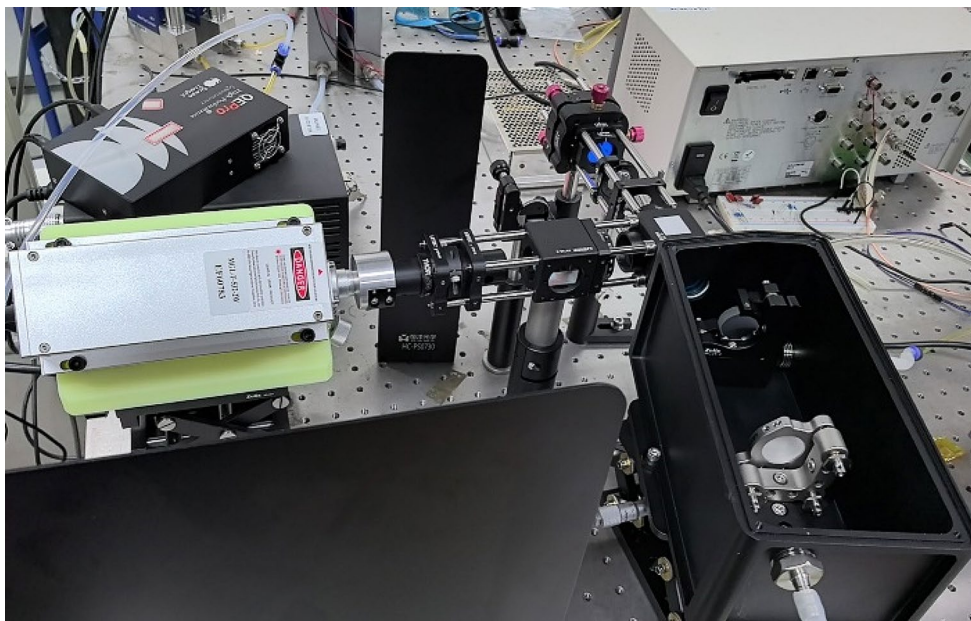


Fig. 1 Schematic diagram of the experimental setup. The green lines represent the laser beam that will be reflected many times in the bidirectional multi-pass cell. The green arrows represent the direction of

the laser beam. The laser light will circulate four specific trips within the multi-pass cell. The orange lines represent the Raman-scattered light, it will be analyzed by the spectrometer

Fig. 2 Instrument photos



at 532 nm and maintains an average reflectivity of 99.4% at 565~675 nm. After undergoing multiple reflections within the multi-pass cell, the laser forms two adjacent foci inside the cell. In the first trip (first round trip) of reflections by adjusting the incident light's angle and the mirror's tilt angle, the incident light's direction vector can coincide with the normal vector of the mirrors in one of the reflections. In this case, the light's incidence angle to the mirror is 0° , the light reverts along the original path and starts the second (multi-pass) trip of reflections. When the laser beam exits the multi-pass cell, it traverses the QW again, transitioning from circularly polarized to P-Polarized. After the P-Polarized laser is split by the PBS, it is reflected by a plane mirror (PM) and starts the third trip (second round trip) of reflections. The laser passes through the PBS again, and repeats the above process, being reflected out of the light path by the optical isolator after four trips of reflections. Compared to a system without a polarization beam-splitting optical path, this system nearly doubles the optical path length and enhances the laser power at the focus significantly, thereby amplifying the Raman scattering signals' intensity.

Collection of Raman scattered light Diverging from the conventional side detection geometry utilized for gas Raman scattering, this system adopts a collinear detection geometry aligned with the laser beam to detect Raman scattering. As the incident laser retraces its path, both forward and backward Raman scatterings produced at the two focal points within the multi-pass cell are multiply reflected by the spherical mirrors and exit in the direction of the incidence laser. Illustrated in Fig. 1, Raman scattering is collimated by the achromatic lens AL_1 before being coupled

into a multi-mode optical fiber (100 μm core diameter) via a 150 mm achromatic lens (AL_2) for subsequent spectral analysis by a spectrometer.

Background noise control Within the collinear detection geometry, the primary sources of background noise are Rayleigh scattering and fluorescence [27] induced by optical components. A dichroic mirror, featuring a cut-off wavelength of 537 nm, allows 0.99% transmission of the 532 nm laser and has an average reflectance of 4% for wavelengths ranging from 550 nm to 800 nm. This configuration effectively blocks the majority of the laser reflected from the multi-pass cell and any fluorescence emitted by optical elements positioned in front of the DM. A long-pass filter (LP) with a cut-off wavelength of 550 nm is positioned before AL_2 . It exhibits a transmission of for 532 nm, effectively filtering out Rayleigh scattering light of the same wavelength as the laser that passes through the dichroic mirror. The remaining background noise mainly stems from fluorescence and Raman scattering produced by optical coatings and components. Enhanced noise control can be achieved by employing mirrors with high reflectivity.

Design of MPC The cavity-enhanced Raman gas detection system is critically reliant on the multi-pass cell, which serves to augment Raman scattering. Our system adopts a bidirectional, near-concentric [28, 29] configuration for the multi-pass cell. This design necessitates greater precision in both the incident light angle and the rotational angle of the reflection mirror, compared to traditional near-concentric multi-pass cells. The conventional ABCD matrix [30–32] method falls short in computing these intricate parameters.

Consequently, we have devised a spatial ray tracing algorithm that leverages vector calculations, coupled with iterative computations in Matlab. This enables the precise calculation of the multi-pass cell parameters for varying numbers of reflections, thus informing the system’s configuration and fine-tuning.

To start, we ascertain the maximum number of reflections permissible within a near-concentric multi-pass cell [29, 33]. This limit is defined by the beam radius r , which corresponds to the solid angle α , and the mirror diameter D , which corresponds to the solid angle β . Given that the spherical mirrors have a focal length f , the maximum number of reflections N can be calculated as:

$$\beta = 2\arcsin\left(\frac{D}{4f}\right) \tag{1}$$

$$\alpha = \arcsin\left(\frac{r}{4f}\right) \tag{2}$$

$$N = \frac{\beta}{\alpha} \tag{3}$$

We then discuss the ray tracing model for multi-pass cell, suppose that LP is the incidence vector of the light and O is the center of the spherical mirror with a curvature radius R , LH can be expressed as follows:

$$|LH| = LO \cdot \frac{LP}{|LP|} \tag{4}$$

The distance from the center of the circle to the incident light can be expressed as:

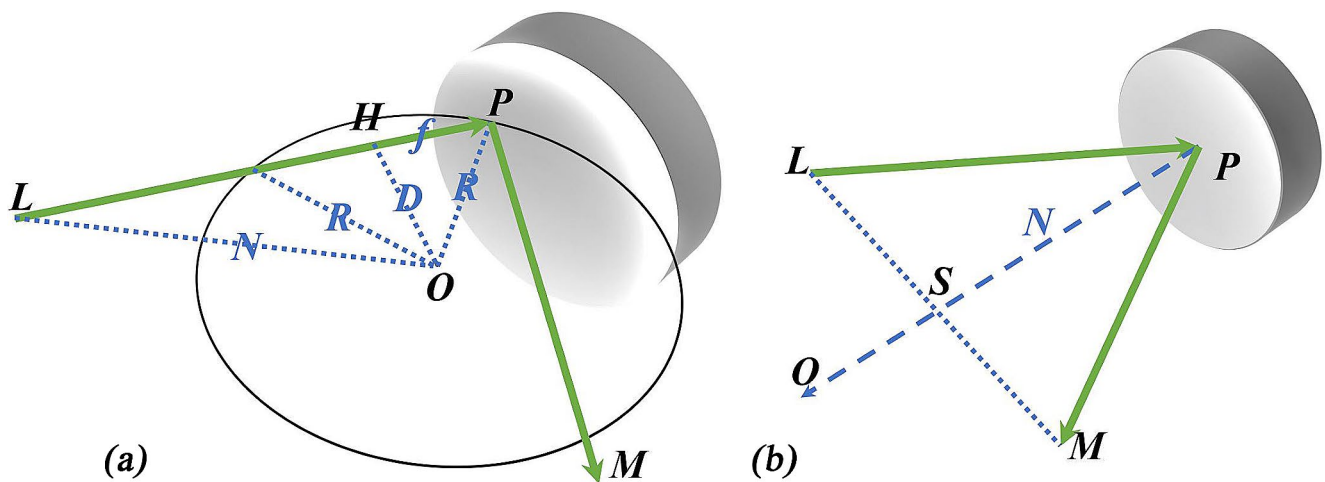


Fig. 3 (a) Schematic diagram of vector reflection model. (b) Calculation of reflected beam direction vector

$$D = \sqrt{N^2 - LH^2} \tag{5}$$

HP can be expressed as:

$$f = \sqrt{R^2 - D^2} = \sqrt{R^2 + LH^2 - N^2} \tag{6}$$

Then the length of the incident laser beam LP is equal to

$$|LP| = |LH| + f \tag{7}$$

As show in Fig. 3 for the direction vector PM of the reflected ray, the normal to the reflecting surface is PO , and the direction vector of the incident ray is LP Here assuming that LP as well as PO are unit vectors then we have:

$$\vec{PM} = \vec{LM} - \vec{LP} \tag{8}$$

$$\vec{LM} = 2(\vec{LP} + \vec{PS}) \tag{9}$$

$$\vec{PS} = -\frac{\vec{LP} \cdot \vec{PO}}{|\vec{PO}|^2} \vec{PO} \tag{10}$$

Then Simplifying Eq. 10 and combining with Eq. 9 and Eq. 8, \vec{PM} can be expressed as:

$$\vec{PM} = \vec{LP} - 2(\vec{LP} \cdot \vec{PO}) \vec{PO} \tag{11}$$

From Eq. 11, we can derive the unit direction vector for the reflected beam. At this juncture, both the coordinates of the reflection point and the direction vector of the reflected beam are ascertained. Treating these as the incident beam parameters for subsequent reflections and recalculating, we can pinpoint the precise coordinates of all reflection points along with the direction vectors of the beams. An additional

step in the iterative process involves verifying whether the ray aligns co-linearly with the mirror's normal to identify suitable parameters for the bi-directional multi-pass cell. Thus, by inputting the incidence point and the direction vector of the initial beam, we can generate a model for the multi-pass cell. Employing vector methods markedly enhances the efficiency of iterative calculations in Matlab without compromising accuracy. Leveraging this model, we have determined the specific parameters for various bi-directional multi-pass cells with reflection number ranging from 7 to 41, the distance d between the beam and the edge of the reflector is set to 0.6 mm, that can be adjusted by the size of the beam diameter. the details of which are depicted in Figs. 4 and 5. The specific data are summarized in Table 1. As show in Fig. 4(i), the diameter of the laser spots on the mirror is 1.1 mm.

3 Results

Firstly, we conducted an experiment to assess the impact of adding PBS and QW (but without PM) on the system's signal intensity. As depicted in Fig. 6, when the total times of reflections is 41 for the multi-pass cell, the signal intensity for the system with PBS and QW (but without PM) was 96.7% of that for the system without PBS and QW. This indicates that the addition of PBS and QW has a minimal impact on the system's signal. However, the signal intensity

for the system with the addition of polarization beam-splitting path (also with PBS and QW) increased by 1.62 times compared to the system without PBS and QW, demonstrating a significant improvement in signal intensity due to the addition of the polarization beam-splitting optical path. Although the addition of PBS and QW results in approximately a 3% reduction in the power of the excitation light, by incorporating the polarizing beam-splitting optical path (with PBS, QW and PM), the effective optical path length can be nearly doubled, and the light intensity at the focal points within the multi-pass cell can be increased significantly, thereby enhancing the Raman scattering signal. Then based on the calculated parameters for various multi-pass cavities, we have engineered cavities with different times of reflections. Ambient air detection was performed under standard atmospheric pressure using multi-pass cavities with varying number of reflections. With a laser power of 600mw and an integration time of 1s. We evaluated the intensity of Raman scattering before and after the addition of polarization beam-splitting optical path. The detection was carried out using the portable and compact QEPro spectrometer by Ocean Optics, which is equipped with a Hamamatsu S7031 type CCD, the slit width of the spectrometer is 25 μ m. As depicted in Fig. 7(a), the purple and blue lines represent the ambient air Raman spectra with and without the polarization beam-splitting optical path, respectively. The Z-axis indicates Raman spectra at different number of reflections, and the side orange curve shows the trend of oxygen Raman

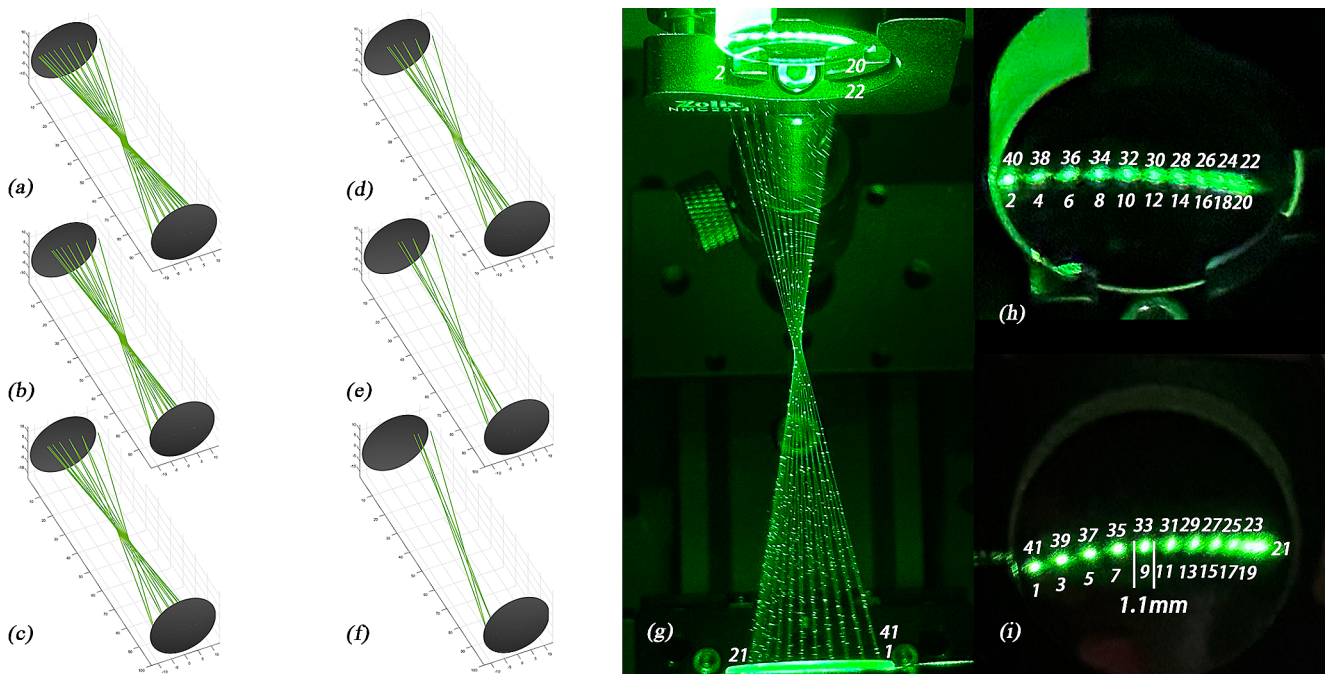


Fig. 4 Simulation results of bidirectional multi-pass cell with different reflection number and actual effect of multi-pass cell with 41 times of reflections. (a) 41 times. (b) 29 times. (c) 23 times. (d) 19 times. (e)

11 times. (f) 7 times. (g) Multi-pass cell. (h) Laser spots on SM₂. (i) Laser spots on SM₁

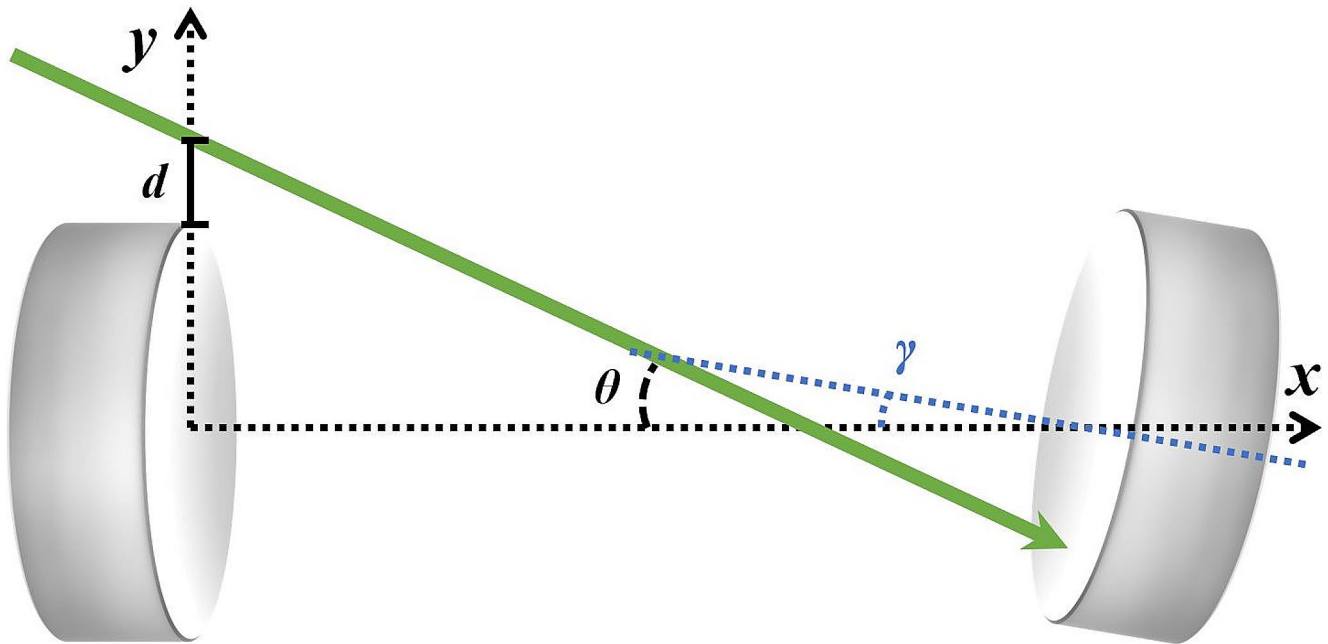


Fig. 5 Parameters of bidirectional multi-pass cell

Table 1 Specific parameters for multi-pass cell

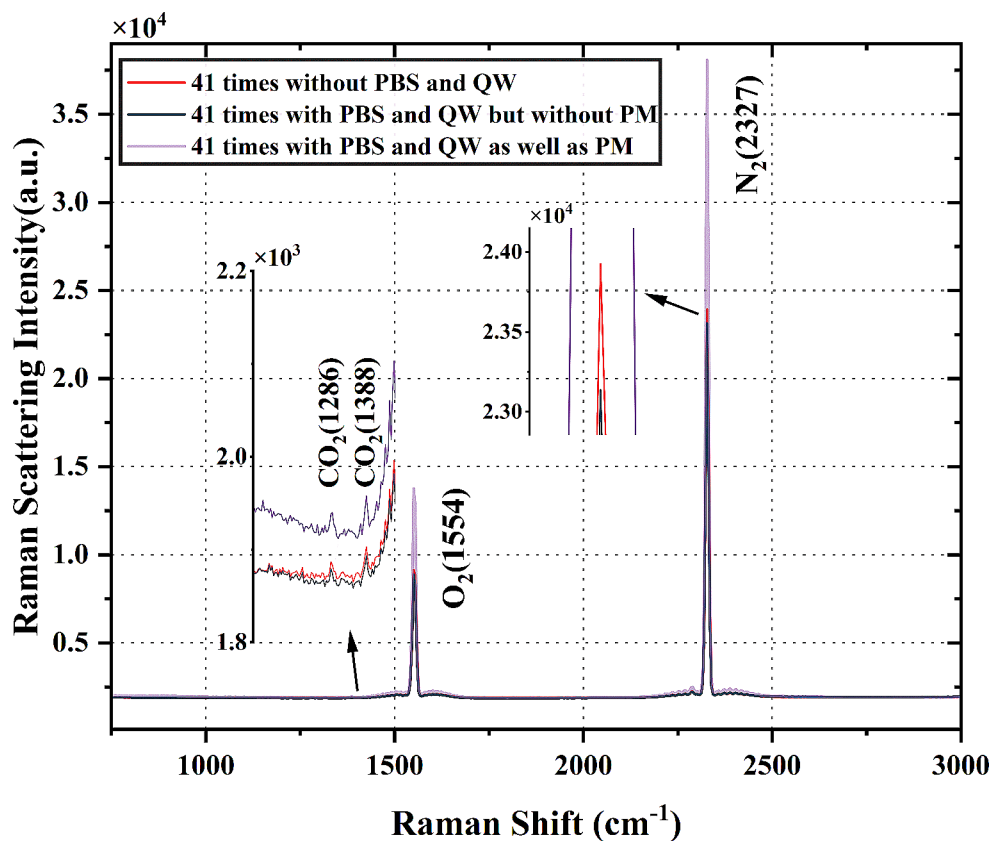
N	$\theta(^{\circ})$	$\gamma(^{\circ})$
41	14.119	0.06
29	14.025	0.09
23	13.58	0.15
19	13.48	0.19
11	13.048	0.39
7	13.678	0.43

scattering intensity with changing number of reflections. Raman scattering signals of CO_2 are observed at 1286 cm^{-1} and 1388 cm^{-1} , O_2 at 1554 cm^{-1} , and N_2 at 2327 cm^{-1} , with signal intensity increasing as the number of reflections in the multi-pass cavity increases. Systems outfitted with polarization beam-splitting optical path exhibit marked enhancements in Raman scattering intensity. The enhancement factor for systems with a multi-pass cell experiencing 11 to 41 times of reflections ranges from 1.68 to 1.5, showing a decreasing trend as the total times of reflections increases. Compared to the signal without multi-pass cavity, the enhancement at 41 times of reflections is 82.8-fold, and with the addition of polarization beam-splitting optical path, it reaches 123-fold. Figure 7(b) shows the Raman spectra where the red, blue, and purple lines correspond to single scattering, 41 times of reflections, and 41 times of reflections with polarization beam-splitting optical path, respectively. Systems with polarization beam-splitting optical path can detect CO_2 in the air, with the Raman scattering signals of CO_2 in laboratory' ambient air becoming discernible at 11 times of reflections. The signal-to-noise ratio (SNR) for CO_2 , calculated using the signal intensity at 1388 cm^{-1} for a

system with 41 times of reflections, is 7.54, where the noise standard deviation σ is 8.52, and the relative signal intensity is 64.2. Moreover, systems with fewer reflections can rival the Raman scattering intensity of systems with a higher number of reflections after introducing polarization beam-splitting optical path. Figure 7 illustrates that a system with 23 times of reflections, once augmented with polarization beam-splitting optical path, has a much higher Raman scattering intensity than a system with 41 times of reflections but without polarization beam-splitting optical path.

To investigate the linear relationship between signal intensity and gas concentration, various concentrations of CO_2 that mix with N_2 were introduced into a sealed gas cell under specific conditions: 23 times of reflections, 600mW laser power, and 1s integration time. A fitting process correlating the signal intensities with the respective gas concentrations was conducted. The results, as illustrated in Fig. 8, demonstrate a remarkable linear relationship between signal intensity and gas concentration, with a correlation coefficient (R^2) of 0.9993. The data represent the average of 120 measurements, with error bars and fitting equation depicted in Fig. 8(b). Using a multi-pass cell with 11 times of reflections, 1 s integration time, and 600mW excitation light power, we conducted the detection on human exhaled gases. As shown in Fig. 9(a), the gas was blown directly into the sealed gas cell by a person through a drying tube. Compared to the ambient air signal, the oxygen signal decreased, whereas the carbon dioxide signal significantly increased. As show in Fig. 9(b), enhancing the laser power to 1800mW and conducting experiments on ambient air with integration times of 1s, 10s, 30s, and 60s, it was established that extending the

Fig. 6 Effect of adding PBS and QW on system signal intensity with 41 times of reflections and the enhancement of system signal intensity by adding polarization beam-splitting optical path



integration time notably enhances the system's SNR. The relative intensity of the CO₂ (1388 cm⁻¹) signal was 4694.8 with a noise standard deviation σ of 43.63 and a SNR of 107.6 at an integration time of 60s.

In order to extend the detection range and reduce the cost of the system we made a Raman spectrometer with a diffraction grating of 1200 L/mm and a Hamamatsu S7031 type CCD (the same model as Ocean Optics' QEPro), and 50 μ m for the slit width of the spectrometer. Utilizing this Raman spectrometer, we conducted experiments on ambient air under specific conditions: 30s integration time, 1800mW laser power and 41 times of reflections. The result is shown in Fig. 10, Raman scattering signals of CO₂, O₂, N₂, CH₄ and H₂O can be observed. The concentration of CH₄ in the ambient air is about 2ppm. The relative intensity of the CH₄ (2917 cm⁻¹) signal was 130.89 with a noise standard deviation σ of 36.3 and the 3 σ detection limit (LOD) of CH₄ is 1.66ppm.

4 Conclusion

In this study, we demonstrate that introducing a polarization beam-splitting optical path to the collinear detection CERS system can effectively amplify gas Raman scattering, catering to the requirement for rapid detection of multi-component gases. Simultaneously, we propose a calculation method for

the parameters of the bidirectional multi-pass cavity, which can guide the design and adjustment of the multi-pass cavity.

Our bidirectional multi-pass cavity, when paired with the polarization beam-splitting optical path, extends the interaction distance between the laser beam and the gas under examination, and amplifies the laser power at the focal point. Importantly, both forward and backward scattering at the two focal points within the multi-pass cavity can be collected, thereby enhancing the collection efficiency of Raman scattering. The multi-pass cavity utilizes two spherical mirrors with a focal length of 25 mm and diameter of 25.4 mm, simplifying the system structure, reducing its physical size, and improving mechanical stability. When combined with the portable spectrometer, this leads to system miniaturization. In comparison to the existing collinear detection geometry, our system, with the addition of polarization beam-splitting optical path, can boost the Raman scattering intensity by 1.5–1.6 times. However, the enhancement effect on the scattering signal diminishes as the number of reflections increases. This is attributable to the increasing of reflection number reducing the laser power and a longer optical path causing a progressive shift in the focal position of the laser beam within the cavity. Additionally, a higher number of reflections may compromise the stability of the optical path. The integration of a polarization beam-splitting optical path enables the multi-pass cavity with fewer reflection numbers to achieve superior detection effects.

Fig. 7 (a) The ambient air Raman scattering intensities before and after the addition of the polarization beam-splitting optical path with different reflection number. The orange curve represents the trend of O₂ Raman scattering intensity with changing reflection numbers. (b) The Raman scattering spectra of ambient air in an open gas cell with 41 times of reflections. (c) The enhancement rate of Raman scattering for the system with a polarization beam-splitting optical path compared to the system without it

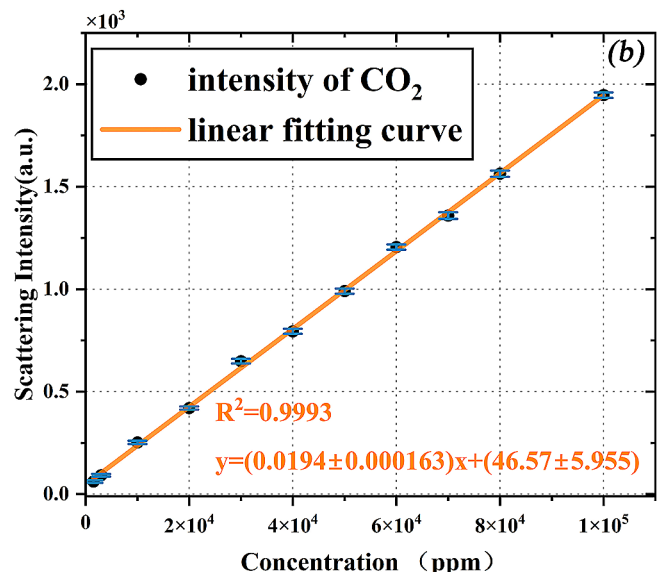
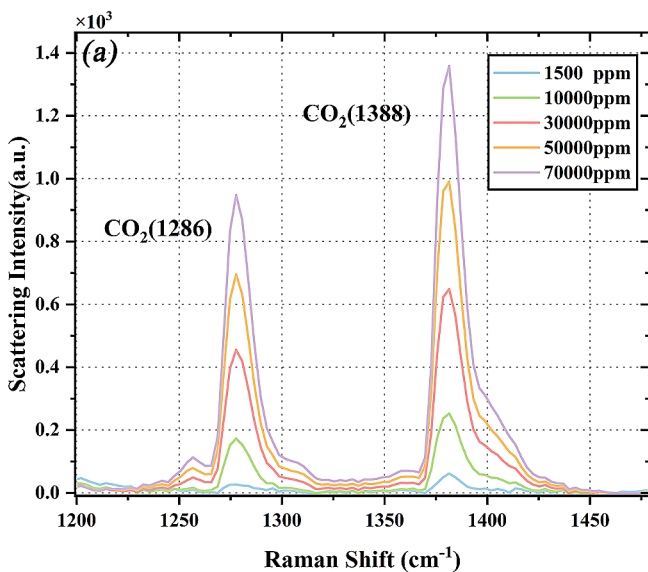
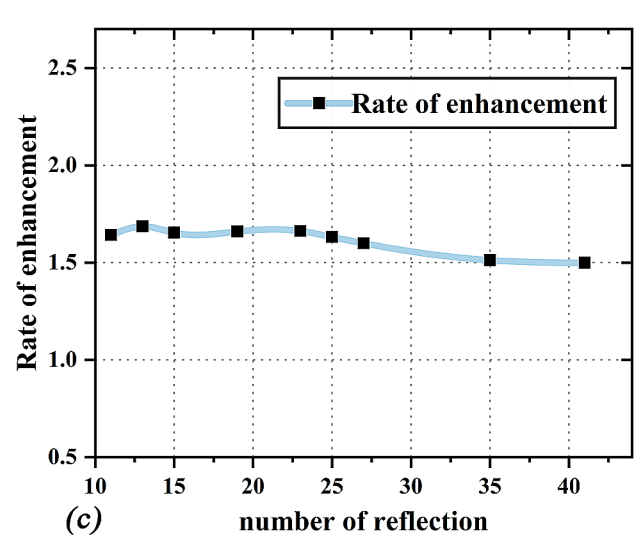
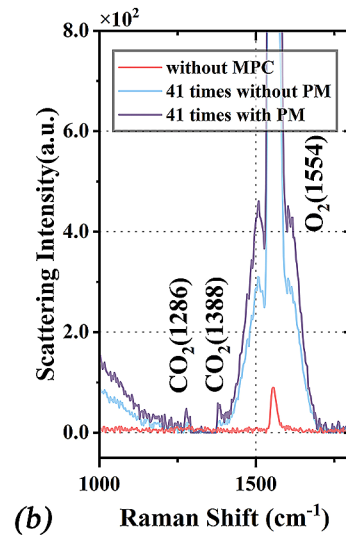
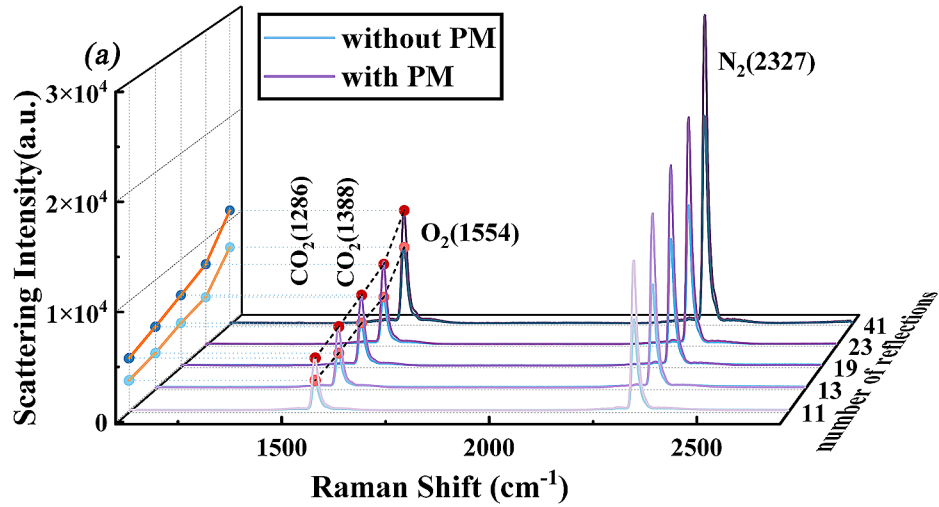


Fig. 8 (a) The intensity of Raman scattering for CO₂ at varying concentrations in a sealed gas cell. (b) The calibration curve of the mean spectrum for this gas cell system with 23 times of reflections

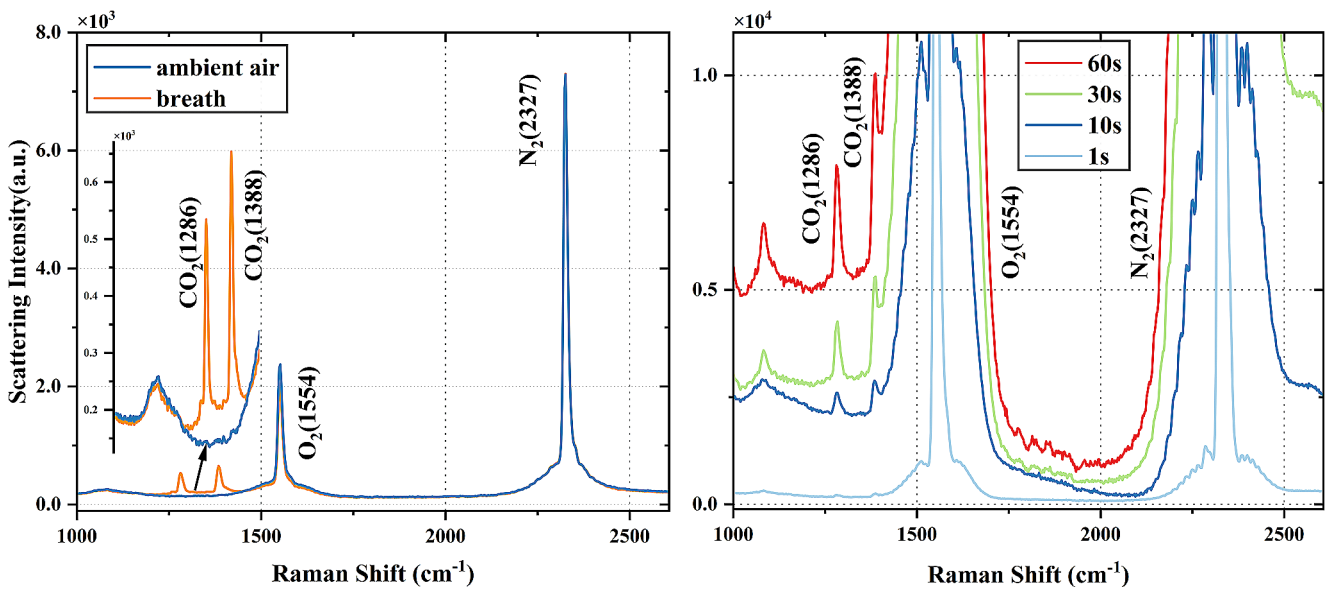
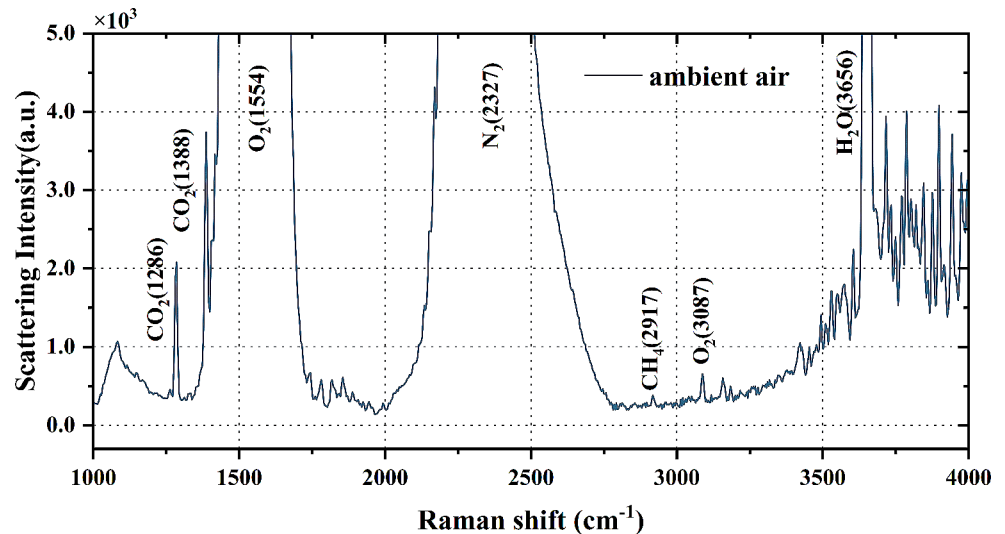


Fig. 9 (a) Raman signal of breath in a sealed gas cell with 11 times of reflections. (b) Raman scattering spectra of ambient air at different integration time without baseline correction

Fig. 10 Raman scattering spectra of ambient air detected using a self-built spectrometer at an integration time of 30s



Future improvements in the Raman scattering intensity of this system could be achieved by reducing the laser wavelength, increasing the gas cell pressure [34, 35], and utilizing mirrors with a higher reflection [2]. We anticipate that this approach could contribute to advancements in greenhouse gas detection and human respiratory component detection. We hope our work on enhancing Raman spectroscopy gas detection sensitivity and designing a bidirectional multi-pass cavity will find utility in future practical applications.

Acknowledgements The authors are grateful to Gaoxuan Wang, Lihui Wang, Yuqi Zhu, Xuhui Huang, Julian Evans for valuable discussion and help.

Author contributions Y.Z. designed the experimental setup. X.Z. participated in the selection of experimental equipment and discussion of experimental details. Y.Z. performed the experiments and analyzed the

data. Y.Z. wrote the software. Y.Z. wrote the manuscript. S.H. supervised the work and finalized the manuscript. All authors have read and agreed to the published version of the manuscript.

Funding Open access funding provided by Royal Institute of Technology. This work was supported by “Pioneer” and “Leading Goose” R&D Program of Zhejiang Province (2022C03051, 2023C03135, 2023C03002, 2023C03083), the National Key Research and Development Program of China (Grant Nos. 2022YFC3601002 and 2022YFC2010003), the Key Research and Development Program of Zhejiang Province (2021C03178), Ningbo Science and Technology Project (2023Z179), and National Natural Science Foundation of China (Grant No.11621101).

Open access funding provided by Royal Institute of Technology.

Data availability The data underlying the results presented in this paper are not publicly available at this time but may be obtained from the authors upon reasonable request.

Declarations

Competing interests The authors declare no competing interests.

Open Access This article is licensed under a Creative Commons Attribution 4.0 International License, which permits use, sharing, adaptation, distribution and reproduction in any medium or format, as long as you give appropriate credit to the original author(s) and the source, provide a link to the Creative Commons licence, and indicate if changes were made. The images or other third party material in this article are included in the article's Creative Commons licence, unless indicated otherwise in a credit line to the material. If material is not included in the article's Creative Commons licence and your intended use is not permitted by statutory regulation or exceeds the permitted use, you will need to obtain permission directly from the copyright holder. To view a copy of this licence, visit <http://creativecommons.org/licenses/by/4.0/>.

References

- S. Hanf et al., Fast and highly sensitive Fiber-enhanced Raman Spectroscopic monitoring of Molecular H₂ and CH₄ for Point-of-care diagnosis of Malabsorption disorders in Exhaled Human Breath. *Anal. Chem.* **87**(2), 982–988 (2015)
- J. Singh, A. Muller, Ambient hydrocarbon detection with an Ultra-low-loss Cavity Raman Analyzer. *Anal. Chem.* **95**(7), 3703–3711 (2023)
- D. Yang et al., Highly sensitive Raman system for dissolved gas analysis in water. *Appl. Opt.* **55**(27), 7744–7748 (2016)
- Y. Xing et al., Voc detections with optical spectroscopy. *Progress Electromagnet. Res.* **173**, 71–92 (2022)
- T. Zhang et al., Elemental mercury sensing by synchronously sweeping two multimode diode lasers. *Appl. Opt.* **59**(11), 3360–3368 (2020)
- G. Wang et al., Compact photoacoustic spectrophone for simultaneously monitoring the concentrations of dichloromethane and trichloromethane with a single acoustic resonator. *Opt. Express.* **30**(5), 7053–7067 (2022)
- Z. Wang et al., Cavity-enhanced Photoacoustic dual-comb Spectroscopy, *Science & Applications, Light*, **13**(1), 11 (2024).
- Z. Wang et al., Doubly resonant sub-ppt photoacoustic gas detection with eight decades dynamic range. *Photoacoustics.* **27**, 100387 (2022)
- L.E. McHale, A. Hecobian, A.P. Yalin, Open-path cavity ring-down spectroscopy for trace gas measurements in ambient air. *Opt. Express.* **24**(5), 5523–5535 (2016)
- Y. Jiang et al., A dual-gas Sensor using Photoacoustic Spectroscopy based on a single Acoustic Resonator. *Appl. Sci.* **11** (2021). <https://doi.org/10.3390/app11115224>
- P. Wang et al., A review of cavity-enhanced Raman spectroscopy as a gas sensing method. *Appl. Spectrosc. Rev.* **55**(5), 393–417 (2020)
- S. Hanf et al., Fiber-enhanced Raman multigas spectroscopy: a versatile tool for environmental gas sensing and breath analysis. *Anal. Chem.* **86**(11), 5278–5285 (2014)
- D. Yan, J. Popp, T. Frosch, Analysis of Fiber-enhanced Raman Gas sensing based on Raman Chemical Imaging. *Anal. Chem.* **89**(22), 12269–12275 (2017)
- J. Wang et al., Analysis of SF₆ decomposed products by fibre-enhanced Raman spectroscopy for gas-insulated switchgear diagnosis. *High. Voltage.* **9**(1), 206–216 (2024)
- J. Gomez Velez, A. Muller, Trace gas sensing using diode-pumped collinearly detected spontaneous Raman scattering enhanced by a multipass cell. *Opt. Lett.*, 2019. **45**(1)
- M. Hippler, Cavity-enhanced Raman Spectroscopy of Natural Gas with Optical Feedback Cw-Diode lasers. *Anal. Chem.* **87**(15), 7803–7809 (2015)
- U. Kc et al., Improved multiple-pass Raman spectrometer. *Appl. Opt.* **50**(24), 4805–4816 (2011)
- P. Wang et al., Multigas Analysis by Cavity-Enhanced Raman Spectroscopy for Power Transformer diagnosis. *Anal. Chem.* **92**(8), 5969–5977 (2020)
- P. Wang et al., Hazardous gas detection by cavity-enhanced Raman Spectroscopy for Environmental Safety Monitoring. *Anal. Chem.* **93**(46), 15474–15481 (2021)
- J. Wang et al., Highly sensitive multi-pass cavity enhanced Raman spectroscopy with novel polarization filtering for quantitative measurement of SF₆ decomposed components in gas-insulated power equipment. *Sens. Actuators B* **380**, 133350 (2023)
- D.V. Petrov, I.I. Matrosov, D.O. Sedinkin, Collection optics for a Raman spectrometer based on the 90 degrees geometry of scattered light collection. *Appl. Opt.* **55**(29), 8293–8295 (2016)
- J.S.G. Velez, A. Muller, Spontaneous Raman scattering at trace gas concentrations with a pressurized external multipass cavity. *Meas. Sci. Technol.*, **32**(4), (2021)
- J. Singh, A. Muller, Isotopic trace analysis of water vapor with multipass cavity Raman scattering. *Analyst.* **146**(21), 6482–6489 (2021)
- Z. Chuan, Y. Anqi, H. Sailing, Lateral Flow Immunoassay Strip based on Confocal Raman Imaging for Ultrasensitive and Rapid Detection of COVID-19 and bacterial biomarkers. *Progress Electromagnet. Res. M.* **120**, 41–54 (2023)
- Z. Xiaoxiao et al., Label-free Assessment of Vericiguat Therapy on Mitochondrial Redox States in Septic mice by Resonance Raman Spectroscopy. *Progress Electromagnet. Res. Lett.* **113**, 119–124 (2023)
- C. Jiao, J. Liao, S. He, An aberration-free line scan confocal raman imager and type classification and distribution detection of microplastics. *J. Hazard. Mater.* **470**, 134191 (2024)
- C. Jiao et al., Noninvasive Raman Imaging for Monitoring Mitochondrial Redox State in septic rats. *Progress Electromagnet. Res.* **175**, 149–157 (2022)
- D. Kaur et al., Multipass cell for molecular beam absorption spectroscopy. *Appl. Opt.* **29**(1), 119–124 (1990)
- D.V. Petrov, Multipass optical system for a Raman gas spectrometer. *Appl. Opt.* **55**(33), 9521–9525 (2016)
- R. Kong et al., Optical design and analysis of a two-spherical-mirror-based multipass cell. *Appl. Opt.* **59**(6), 1545–1552 (2020)
- J. Liu et al., Generalized optical design and optimization of multipass cells with independent circle patterns based on the Monte Carlo and Nelder-Mead simplex algorithms. *Opt. Express.* **29**(13), 20250–20261 (2021)
- Y. Liu, Y. Ma, Advances in multipass cell for absorption spectroscopy-based trace gas sensing technology [Invited]. *Chin. Opt. Lett.*, **21**(3), (2023)
- X. Li et al., Near-confocal cavity-enhanced Raman spectroscopy for multitrace-gas detection. *Opt. Lett.* **33**(18), 2143–2145 (2008)
- D.V. Petrov, I.I. Matrosov, Pressure dependence of the Raman signal intensity in high-pressure gases. *J. Raman Spectrosc.* **48**(3), 474–478 (2017)
- D.V. Petrov et al., Effects of pressure and composition on Raman spectra of CO-H₂-CO₂-CH₄ mixtures. *Spectrochim. Acta Part A Mol. Biomol. Spectrosc.* **215**, 363–370 (2019)

Publisher's Note Springer Nature remains neutral with regard to jurisdictional claims in published maps and institutional affiliations.